

ChemComm

Accepted Manuscript



This is an *Accepted Manuscript*, which has been through the Royal Society of Chemistry peer review process and has been accepted for publication.

Accepted Manuscripts are published online shortly after acceptance, before technical editing, formatting and proof reading. Using this free service, authors can make their results available to the community, in citable form, before we publish the edited article. We will replace this *Accepted Manuscript* with the edited and formatted *Advance Article* as soon as it is available.

You can find more information about *Accepted Manuscripts* in the [Information for Authors](#).

Please note that technical editing may introduce minor changes to the text and/or graphics, which may alter content. The journal's standard [Terms & Conditions](#) and the [Ethical guidelines](#) still apply. In no event shall the Royal Society of Chemistry be held responsible for any errors or omissions in this *Accepted Manuscript* or any consequences arising from the use of any information it contains.

COMMUNICATION

Hydrothermal growth of highly oriented single crystalline Ta₂O₅ nanorod arrays and their conversion to Ta₃N₅ for efficient solar driven water splitting

Cite this: DOI: 10.1039/x0xx00000x

Received 00th January 2012,
Accepted 00th January 2012

DOI: 10.1039/x0xx00000x

www.rsc.org/

Zixue Su,^a Lei Wang,^a Sabina Grigorescu,^a Kiyoungh Lee,^a and Patrik Schmuki^{a,b,*}

We grow vertically aligned single crystalline Ta₂O₅ nanorod arrays that can be converted to a Ta₃N₅ nanorod array by nitridation. Combined with cobalt phosphate (Co-Pi) as a co-catalyst, such Ta₃N₅ nanorod photoanodes can yield photocurrent densities of ~3.6 mA cm⁻² at 1.23 V_{RHE}, and ~8.2 mA cm⁻² at 1.59 V_{RHE} under AM 1.5G (100 mW cm⁻²).

Hydrogen production via photoelectrochemical (PEC) water splitting is receiving strongly increased attention in the past years, as a means to convert solar energy directly into an ideal clean fuel. After the first report by Fujishima and Honda in 1972¹ on hydrogen generation using TiO₂ as a photocatalyst, considerable efforts have been dedicated to tailor the electronic properties and morphology of photocatalysts to improve the efficiency of PEC water splitting.¹⁻⁴ With a band gap of about 2.1 eV and suitable band positions, Ta₃N₅ can utilize a large portion of the solar spectrum (< 600 nm), and is considered to be one of the most promising photoanodes for solar water splitting, as Ta₃N₅ can reach a theoretical maximum of ≈16% light conversion under AM 1.5G irradiation.⁵⁻⁷ Various methods such as morphology control, doping and the use of charge transfer catalysts have been introduced to improve the performance of Ta₃N₅ based PEC cells.⁸⁻¹⁰ Additionally, structuring of semiconductors at the nanoscale is widely used, not only to provide abundant surface reaction sites but also to aid transport and separation of photoexcited charge carriers.² Namely vertically aligned one-dimensional (1D) nanorod arrays are considered to be very promising and efficient structures for energy harvesting systems.

A common path to synthesize Ta₃N₅ is nitridation of Ta₂O₅ by a high temperature NH₃ treatment. Previous reports on Ta₃N₅ nanorod fabrication use hydrothermal methods with Ta powders,¹¹ or a vapor-phase hydrothermal (VPH) process,¹² or use porous anodic alumina (PAA) as a template for through mask anodization with a two-step anodization process, to grow the Ta₂O₅ precursors.¹³ Subsequently

these structures are nitride, and frequently co-catalyst decorated and doped for an optimized water splitting performance. A current record efficiency is held by PAA template oxide rods after modification to Ba doped Co-Pi/Ta₃N₅ nanorods; corresponding photoanodes yielded a photocurrent of 6.3 mA cm⁻² at 1.23 V_{RHE} in 0.5 M K₂HPO₄ solution with a pH of 13.¹³ For Ta₃N₅ nanorods produced by the VPH method and modified with Co(OH)_x, a photocurrent density for water splitting of 2.8 mA cm⁻² at 1.23 V_{RHE} under AM 1.5 simulated sunlight was obtained.^{12a} In the present work, we introduce an alternative facile, template free hydrothermal method for the fabrication of vertically aligned Ta₃N₅ nanorods. For this we grow single crystalline Ta₂O₅ aligned nanorod arrays on the surface of Ta foils by a direct solution-immersion approach, and then convert these oxide structures to nitride.

To grow the Ta₂O₅ nanorod arrays as shown in the scanning electron microscopy (SEM) images of Fig. 1a and b, we immersed Ta foils in a 250 ml Teflon-lined autoclave into 100 ml 0.1 M HF and 0.59 M H₂O₂ solution, which was then heated to 240 °C and kept for 24 h. After synthesis, a densely packed nanorod array is obtained that uniformly covers the entire surface of the Ta foil substrate. The nanorods grow perpendicularly from the Ta substrate on a base oxide layer with a thickness of about 0.7 μm. The average length and diameter of the nanorods are about 0.6 μm and 100 nm, respectively.

Figure 1c displays the XRD pattern of Ta₂O₅ nanorod arrays grown on the Ta surface. All the diffraction peaks can be assigned to the Ta substrate and the orthorhombic phase of Ta₂O₅ (JCPDS No. 01-089-2843, a=0.620 nm, b=0.366 nm, c=0.389 nm). It is impressive that only crystal planes parallel to the (001) plane show diffraction peaks, and other diffraction peaks which usually appear in a powder diffraction of an orthorhombic phase of Ta₂O₅, such as (110), (200), and (111) peaks are absent. This indicates that the Ta₂O₅ nanorod arrays grown are single crystalline and highly oriented, with a growth axis in the [001] direction perpendicular to the Ta substrate.

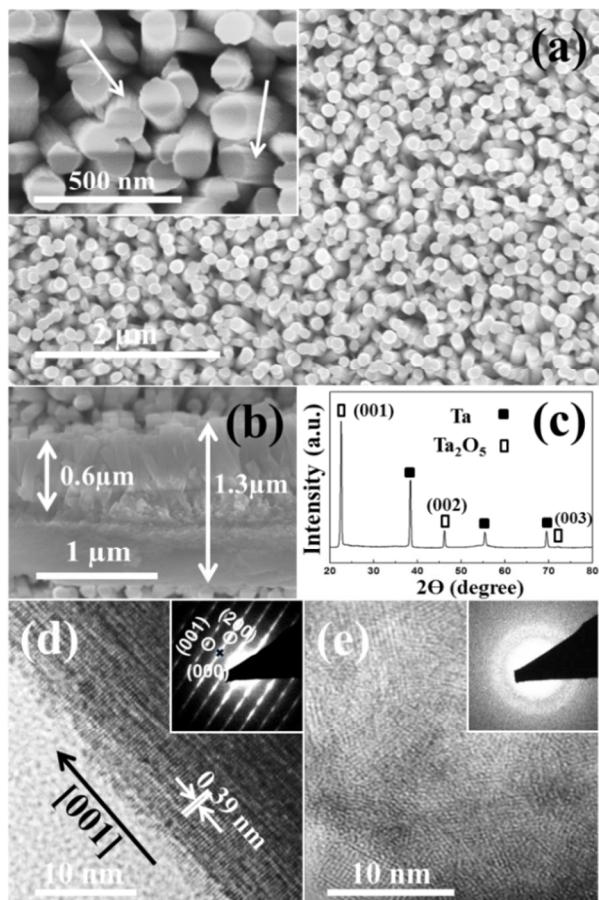
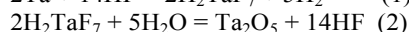


Figure 1. Top view (a) and cross-sectional view (b) SEM images, and (c) corresponding XRD pattern of vertically aligned Ta₂O₅ nanorod arrays grown hydrothermally in 0.1 M HF and 0.59 M H₂O₂ at 240 °C for 24 h with a solution filling factor of 40%. HRTEM images in (d) and (e) show the microstructures of a single nanorod and the base oxide layer of the hydrothermally grown Ta₂O₅ films. The insets in (d) and (e) are corresponding SAED patterns.

High resolution transmission electron microscopy (HRTEM) images and a corresponding selected area electron diffraction (SAED) pattern of a typical single nanorod of Ta₂O₅ are shown in Figure 1d. The fringes with an interspace of 0.39 nm match well with the (001) crystal planes of orthorhombic Ta₂O₅, confirming that the nanorods were grown in the (001) direction. The SAED pattern with disperse diffraction spots periodically arranged in two dimensions confirms that the nanorod is single crystalline but contains some stacking faults. Typical HRTEM image of the base oxide layer underneath the nanorod arrays in Figure 1e shows that the oxide layer composes of many nanocrystallites which show only an amorphous characteristic diffuse ring in the SAED pattern due to the very small size of the nanocrystals. Many micropores with a size of about 1.5 nm are revealed by low magnification TEM image in Figure S1.

The main chemical reactions in the autoclave can be written as:¹¹



The concentration of H₂TaF₇ which gradually increases with the etching of Ta foil has significant influence on the dissolution and growth of Ta₂O₅ films as described in equation

(2). At low H₂TaF₇ concentration, the formed Ta₂O₅ can be readily dissolved back to H₂TaF₇ by excess HF solution according to the back reaction of equation (2). In this work, no oxide layer was observed on the Ta substrate after 6 h reaction. After this initial incubation period, microporous nanocrystalline Ta₂O₅ films are able to grow on the Ta substrate as an appropriate H₂TaF₇ concentration is established. Single crystal Ta₂O₅ nanorods grow probably from nanocrystalline Ta₂O₅ nuclei. To minimize the surface energy, Ta₂O₅ nanorods tend to grow slowly along the [001] direction via a thermodynamically controlled process, consistent with previous reported hydrothermal growth of dispersed branched Ta₂O₅ nanorods.¹¹ Since the growth and dissolution of the oxide compete with each other according to the forward and back reaction of equation (2), clear stripes can be observed on the wall of all the nanorods as pointed by arrows in Figure 1a. This explains how single crystalline Ta₂O₅ nanorod arrays grow in diameter and length after 12 h and 24 h of reaction. The morphology of the 12 h grown Ta₂O₅ films is shown in Figure 2a and c. As the reaction continues, the growth rate of Ta₂O₅ increased accordingly with further increasing concentration of H₂TaF₇, which finally facilitates the fast growth of base oxide layer consisting of Ta₂O₅ nanocrystallites and suppresses the single crystal nanorod growth. The dissolution of the single crystal nanorods by the solution may cause thinning of the nanorods and induce disorder of the nanorod alignment. Figure 2b and d show that the 48 h grown samples have much thicker base oxide layer, but with smaller, shorter and less ordered nanorod arrays compared to the 24 h grown sample in Figure 1. The influence of various experimental parameters such as pre-oxidation of the Ta, Ta foil size, and solution amount in the autoclave on the morphologies of Ta₂O₅ film were studied as outlined in the supplementary information. These experiments further support the above suggestion that hydrothermal growth of Ta₂O₅ films on Ta foils is greatly determined by the H₂TaF₇ concentration.

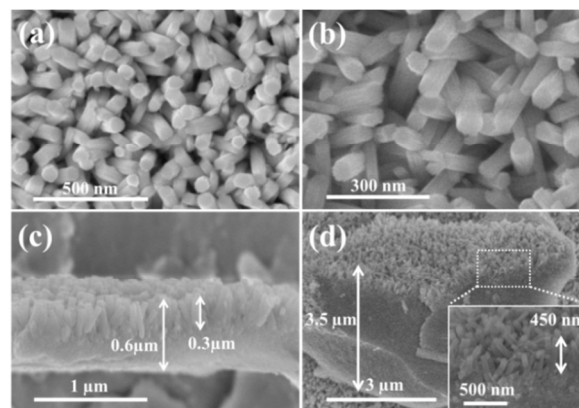


Figure 2. Top view (a,b), and cross-sectional view (c,d) SEM images of Ta₂O₅ nanorod arrays grown hydrothermally in 0.1 M HF and 0.59 M H₂O₂ at 240 °C for 12 h (a,c) and 48 h (b,d).

For nitridation, typical Ta₂O₅ nanorod arrays grown by 24 h hydrothermal reaction (as shown in Fig. 1a) were placed into a quartz tube, which were then heated to 1000 °C for 2 h with a NH₃ flow of about 200 sccm. XRD analysis of the products revealed that the Ta₂O₅ films had been converted to tantalum nitrides completely, the structure in line with hexagonal TaN (JCPDS No. 01-089-5197) and the major phase, orthorhombic Ta₃N₅ (JCPDS No. 01-079-1533) as shown in Figure 3. The

densities of TaN, Ta₃N₅ and Ta₂O₅ are $\sim 15 \text{ g cm}^{-3}$,¹⁴ 9.8 g cm^{-3} and 8.2 g cm^{-3} ,¹⁵ corresponding to a Ta atomic density of $\sim 0.0769 \text{ mol cm}^{-3}$, $0.0482 \text{ mol cm}^{-3}$ and $0.0371 \text{ mol cm}^{-3}$ respectively. This is the origin of the observed significant volume contraction during nitridation of Ta₂O₅. As can be seen from the FE-SEM images in Figure 3, the diameter and length of Ta₃N₅ nanorods are much smaller than for the original Ta₂O₅ nanorods shown in Figure 1. The base oxide layer underneath the nanorod arrays changed to a mesoporous nanoparticle layer with a lower thickness, as well. The average size of the nanoparticles is about 30 nm, while the average pore size is about 10 nm. The HRTEM image shown in Figure 3c reveals a mesoporous nature of the Ta₃N₅ nanorods. Both the mesoporous 1D nanorod arrays and the mesoporous nanoparticle layers of Ta₃N₅ can act as efficient photocatalysts for the PEC water splitting due to their high specific surface areas and good charge transport properties.

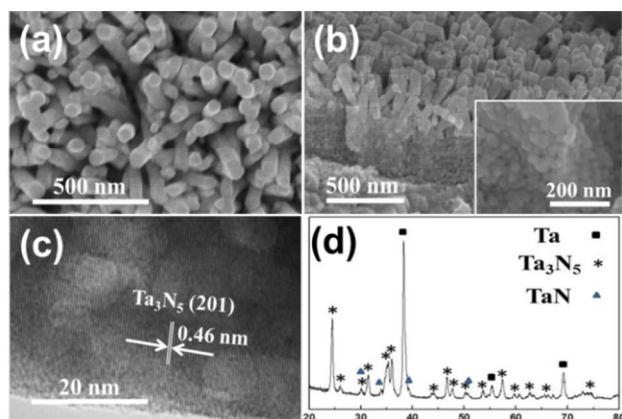


Figure 3. Top-view (a) and cross-sectional view (b) SEM images of Ta₃N₅ nanorod arrays obtained by 2 h nitridation at 1000 °C of Ta₂O₅ nanorod arrays grown hydrothermally in 0.1 M HF and 0.59 M H₂O₂ at 240 °C for 24 h with a filling factor of 40%. The inset of (b) is an enlarged image of the nanoparticle layer. (c) Typical HRTEM image of a single nanorod. (d) XRD pattern of the nanorod arrays.

In the PEC water splitting process, when using Ta₃N₅ as the photoanode, photo-generated holes with strong oxidative ability tend to oxidize the photoanode if they cannot be effectively transferred away from the anode/electrolyte interface,¹⁶ which significantly impairs the stability of the photoanode. Surface modification with co-catalysts such as IrO₂, Co₃O₄, Co(NO₃)₂, Co-Pi, and Co(OH)_x are reported to stabilize the Ta₃N₅ photoanode and improve the water splitting efficiency significantly.^{13,17-19} To deposit a layer of Co(OH)_x nanoparticles on Ta₃N₅ nanorod arrays as a co-catalyst, the Ta₃N₅ nanorod array films were simply immersed in a mixed solution of CoSO₄ and NaOH for 25 min, then rinsed by deionized water and finally dried in N₂. In comparison, the Co-Pi co-catalyst was loaded on the nanorod surface by electrodeposition in a solution of 0.5 mM Co(NO₃)₂ in 0.1 M potassium phosphate buffer at pH=7 at 1 V versus Ag/AgCl for 8 min. As shown in Figure 4, the Co(OH)_x treated Ta₃N₅ nanorod photoanode yields a photocurrent density of $\sim 1.5 \text{ mA cm}^{-2}$ at 1.23 V_{RHE}, which increases to $\sim 10.4 \text{ mA cm}^{-2}$ at 1.59 V_{RHE}. For the Co-Pi/Ta₃N₅ photoanode, typical photocurrent densities of $\sim 3.6 \text{ mA cm}^{-2}$ at 1.23 V_{RHE}, and $\sim 8.2 \text{ mA cm}^{-2}$ at 1.59 V_{RHE} were obtained. Some fluctuation in the initial spike height is just due to the use of a comparably slow sampling rate (data

acquisition). In both cases the appearance of spike-like initial transients depends on the applied potential, indicating that at lower potentials, photogenerated electrons and holes show considerable recombination.

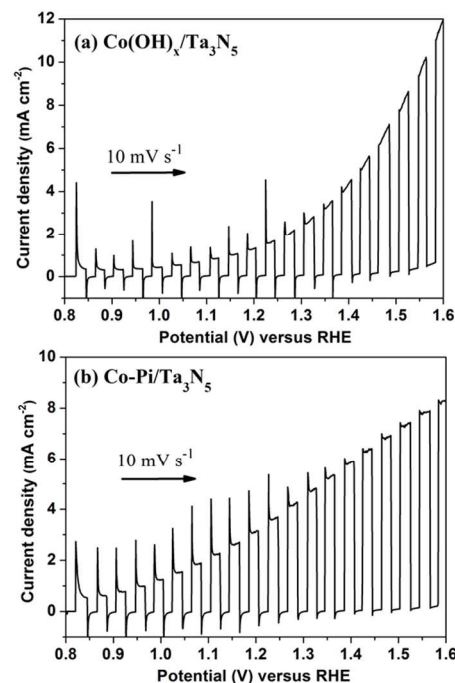


Figure 4. Current-potential curves of PEC water splitting cell with a photoanode of Ta₃N₅ nanorod arrays obtained from 2 h nitridation at 1000 °C of 24 h grown Ta₂O₅ nanorod arrays modified by (a) Co(OH)_x and (b) Co-Pi. All curves were measured in aqueous KOH solution (pH=13.7) under chopped AM 1.5G simulated sunlight, with a scan rate of 10 mV s⁻¹ from negative to positive.

The PEC water splitting performance of Ta₃N₅ nanorods after different hydrothermal time is shown in Figure S2. It was found that an increase in the time of hydrothermal growth of Ta₂O₅ to 48 h or a decrease to 12 h in both cases, the performance of the corresponding Ta₃N₅ nanorods decreases considerably. The 12 h grown nanorods and sub-spongy layer seem too short to achieve an efficient visible light absorption (400 nm < λ < 700 nm), especially when the volume contraction during nitridation is taken into consideration. The oxide layer for the 48 h grown sample is too thick for an efficient charge transport. On the other hand, the TEM and SAED pattern taken in the sponge layer (Fig. S3) identify the presence of TaN in this structure. TaN, in turn, has been reported to be detrimental for the water oxidation performance of Ta₃N₅ photoanode.²⁰

Compared with the Co(OH)_x decoration, the electrode with the Co-Pi treatment exhibits not only an onset potential that is negatively shifted but also an improved photocurrent. The Co(OH)_x/Ta₃N₅ electrode shows relatively stronger spike-like transients, but compared to literature reported on Ta₃N₅ nanorod with Co(OH)_x decoration¹², our electrode shows a higher saturation photocurrent ($\sim 10.4 \text{ mA cm}^{-2}$ at 1.59 V_{RHE}).

Among all the currently available Ta₃N₅ photoanodes reported, thermal Ta₃N₅ films after removal of the surface passivation layer as reported by Zou et al.¹⁷ and templated aligned Ta₃N₅ nanorod arrays doped by barium as reported by Domen et al.¹³ currently represent, to the best of our

knowledge, the highest solar photocurrent densities. In the first case, the photoanode has a photocurrent density of $\sim 5.5 \text{ mA cm}^{-2}$ at $1.23 \text{ V}_{\text{RHE}}$ and a saturated photocurrent density of $\sim 8 \text{ mA cm}^{-2}$ at $1.60 \text{ V}_{\text{RHE}}$.¹⁷ The barium doped Ta_3N_5 nanorod photoanodes¹³ have a high photocurrent density at low bias region after optimized loading of Co-Pi by photo-assisted electrodeposition, e.g., $\sim 4.75 \text{ mA cm}^{-2}$ at $0.9 \text{ V}_{\text{RHE}}$ and $\sim 6.7 \text{ mA cm}^{-2}$ at $1.23 \text{ V}_{\text{RHE}}$.

For our structure, while the onset conversion efficiency in previous work is slightly lower than in the best reported case, the saturation solar photocurrent density of our Ta_3N_5 nanorod photoanode is higher than the highest value reported for Ta_3N_5 based photoanodes.^{13,17} This illustrates the high potential of the present approach, namely if optimization of the co-catalyst loading is achieved, to improve the performances in lower applied voltage region.

In summary, highly oriented single crystalline Ta_2O_5 nanorod arrays were successfully grown on Ta foils by a facile hydrothermal method without any template. Upon nitridation in NH_3 atmosphere at $1000 \text{ }^\circ\text{C}$ for 2 h, the grown nanorods were converted to Ta_3N_5 nanorod arrays that represent highly efficient anodes for PEC water splitting. By deposition of a layer of $\text{Co}(\text{OH})_x$ nanoparticles on Ta_3N_5 nanorod arrays as co-catalyst, we obtained solar photocurrents of 1.5 mA cm^{-2} at $1.23 \text{ V}_{\text{RHE}}$ and 10.4 mA cm^{-2} at $1.59 \text{ V}_{\text{RHE}}$; the latter is the highest values reported for Ta_3N_5 photoanodes to the best of our knowledge. Ta_3N_5 nanorods modified by electrodeposition of Co-Pi yield typical solar photocurrents of 3.6 mA cm^{-2} at $1.23 \text{ V}_{\text{RHE}}$ and 8.2 mA cm^{-2} at $1.59 \text{ V}_{\text{RHE}}$. In future studies, optimization of the experimental conditions is required to control the growth of Ta_2O_5 and the subsequent Ta_3N_5 nanorod arrays to strengthen the advantage of the 1D nanorod structure, and more importantly, co-catalyst treatments will need to be optimized to lower the onset potential of photocurrent and the efficiency under low bias conditions.

We thank Dr. Mirza Mackovic and the center for nanoanalysis and electron microscopy at the university of Erlangen-Nuremberg for help with the TEM analysis. The authors would like to acknowledge DFG and the DFG cluster of excellence "Engineering of Advanced Materials" (EAM) for the financial support.

Notes and references

^a Department of Materials Science and Engineering, WW4-LKO, University of Erlangen-Nuremberg, Martensstr. 7, D-91058 Erlangen, Germany.

* Corresponding Author: schmuki@ww.uni-erlangen.de (P. Schmuki)

^b Department of Chemistry, King Abdulaziz University, Jeddah, Saudi Arabia.

Electronic Supplementary Information (ESI) available: [details of any supplementary information available should be included here]. See DOI: 10.1039/c000000x/

1 A. Fujishima, K. Honda, *Nature* 1972, **238**, 37.

- 2 Z. Fan, H. Razavi, J.-W. Do, A. Moriwaki, O. Ergen, Y.-L. Chueh, P. W. Leu, J. C. Ho, T. Takahashi, L. A. Reichertz, S. Neale, K. Yu, M. Wu, J. W. Ager, A. Javey, *Nat. Mater.* 2009, **8**, 648.
- 3 C. Chaneliere, J. L. Autran, R. A. B. Devine, B. Bolland, *Mater. Sci. Eng.* 1998, **R22**, 269.
- 4 Y. Takahara, J. N. Kondo, T. Takata, D. L. Lu, K. Domen, *Chem. Mater.* 2001, **13**, 1194.
- 5 W. J. Chun, A. Ishikawa, H. Fujisawa, T. Takata, J. N. Kondo, M. Hara, M. Kawai, Y. Matsumoto, K. Domen, *J. Phys. Chem. B* 2003, **107**, 1798.
- 6 M. Hara, E. Chiba, A. Ishikawa, T. Takata, J. N. Kondo, K. Domen, *J. Phys. Chem. B* 2003, **107**, 13441.
- 7 A. B. Murphy, P. R. F. Barnes, L. K. Randeniya, I. C. Plumb, I. E. Grey, M. D. Horne, J. A. Glasscock, *Int. J. Hydrogen Energy* 2006, **31**, 1999.
- 8 Y. Lin, Y. Xu, M. T. Mayer, Z. I. Simpson, G. McMahon, S. Zhou, D. Wang, *J. Am. Chem. Soc.* 2012, **134**, 5508.
- 9 B. D. Alexander, P. J. Kulesza, I. Rutkowska, R. Solarska, J. Augustynski, *J. Mater. Chem.* 2008, **18**, 2298.
- 10 Y. Kado, C.-Y. Lee, K. Y. Lee, J. Müller, M. Moll, E. Spiecker, P. Schmuki, *Chem. Commun.* 2012, **48**, 8685.
- 11 J. Y. Duan, W. D. Shi, L. L. Xu, G. Y. Mou, Q. L. Xin, J. G. Guan, *Chem. Commun.* 2012, **48**, 7301.
- 12 (a) C. Zhen, L. Z. Wang, G. Liu, G. Q. (Max) Lu, H. M. Cheng, *Chem. Commun.* 2013, **49**, 3019. (b) J. G. Hou, Z. Wang, C. Yang, H. J. Cheng, S. Q. Jiao, H. M. Zhu, *Energy Environ. Sci.* 2013, **6**, 3322.
- 13 (a) Y. B. Li, T. Takata, D. Cha, K. Takanabe, T. Minegishi, J. Kubota, K. Domen, *Adv. Mater.* 2013, **25**, 125. (b) Y. B. Li, L. Zhang, A. Torres-Pardo, J. M. Gonzalez-Calbet, Y. H. Ma, P. Oleynikov, O. Terasaki, S. Asahina, M. Shima, D. Cha, L. Zhao, K. Takanabe, J. Kubota, K. Domen, *Nat. Comm.* 2013, **4**, 2566.
- 14 G. M. Matenoglou, L. E. Koutsokeras, Ch. E. Lekka, G. Abadias, S. Camelio, G. A. Evangelakis, C. Kosmidis, P. Patsalas, *J. Appl. Phys.* 2008, **104**, 124907.
- 15 B. A. Pinaud, P. C. K. Vesborg, T. F. Jaramillo, *J. Phys. Chem. C* 2012, **116**, 15918.
- 16 D. Yokoyama, H. Hashiguchi, K. Maeda, T. Minegishi, T. Takata, R. Abe, J. Kubota, K. Domen, *Thin Solid Films* 2011, **519**, 2087.
- 17 M. X. Li, W. J. Luo, D. P. Cao, X. Zhao, Z. S. Li, T. Yu, Z. G. Zou, *Angew. Chem. Int. Ed.* 2013, **52**, 11016.
- 18 H. X. Dang, N. T. Hahn, H. S. Park, A. J. Bard, C. B. Mullins, *J. Phys. Chem. C* 2012, **116**, 19225.
- 19 Y. Q. Cong, H. S. Park, S. J. Wang, H. X. Dang, F. F. Fan, C. B. Mullins, A. J. Bard, *J. Phys. Chem. C* 2012, **116**, 14541.
- 20 E. Nurlaela, S. Ould-Chikh, M. Harb, S. D. Gobbo, M. Aouine, E. Puzenat, P. Sautet, K. Domen, J.-M. Basset, K. Takanabe, *Chem. Mater.* 2014, **26**, 4812.